Evaluation of Equi-biaxial Strength of Thin SiC Coatings Using Ring-on-Ring Testing and Digital Image Correlation

Sola Iwamoto [1,2], Sosuke Kondo [2,*], Hirokazu Katsui [3], Kazuya Shimoda [4], Hao Yu [2], Yasuyuki Ogino [2], Ryuta Kasada [2]

[1] Department of Quantum Science and Energy Engineering, Graduate School of Engineering, Tohoku University, Sendai, Miyagi, Japan

[2] Institute for Materials Research, Tohoku University, Sendai, Miyagi, Japan

[3] National Institute of Advanced Industrial Science and Technology, Nagoya, Aichi, Japan

[4] Research Center for Structural Materials, National Institute for Materials Science, Tsukuba, Ibaraki, Japan

Correspondence

Sosuke Kondo, Institute for Materials Research, Tohoku University, 2-1-1 Katahira, Aoba-ku, Sendai, Miyagi 980-8577, Japan

E-mail: sosuke.kondo.d4@tohoku.ac.jp

Abstract

To assess the strength of coatings under multi-axial stress conditions, a method was developed to evaluate the biaxial strength of thin silicon carbide (SiC) coatings using a Ring-on-Ring test. A graphite substrate was used as an intermediary to transmit stress from the load ring to the coated specimen, and the thin coating was subjected to a uniform equi-biaxial stress. The strain in the thin film was continuously monitored using digital image correlation, allowing the identification of the time at which and when the initial crack occurred; the stress applied to the loading area at time was determined to be the fracture strength of the thin SiC films. The obtained fracture strength ranged from 209 to 1014 MPa and was dependent on specimen volume. Notably, the thinnest specimen exhibited the highest strength, whereas the strengths of thicker specimens approached previously reported bulk strengths.

1. Introduction

Silicon carbide (SiC) and SiC fiber-reinforced SiC matrix composites (SiC/SiC), which are renowned for their exceptional properties, including high strength, high- temperature stability, excellent oxidation resistance, and wear resistance, are deemed to possess superior fundamental properties among engineering ceramics.[1-3] These materials are expected to be applied in aircraft engine components, fusion reactor blankets, and nuclear reactor fuel claddings.[3-6] The manufacturing methods for SiC/SiC composites are primarily classified into chemical vapor infiltration (CVI), polymer infiltration and pyrolysis (PIP), and melt infiltration (MI).[3] However, PIP-manufactured SiC/SiC composites often exhibit 10–20 % residual pores and precipitation of excess elements.[3] Similarly, the MI method results in the precipitation of residual Si, C, and additives as secondary phases, which reduces oxidation and creep resistance.[3] Pore formation inside the preform remains a concern even in the CVI method, which is known to produce the highest-purity materials among these manufacturing methods. Recent advancements have been made in the development of small modular reactor cores using additive manufacturing (AM).[7,8] However, the presence of residual impurities from the thermal decomposition process, such as SiO_2, may potentially serve as initiation points for corrosion in high-temperature and high-pressure cooling water applications.[9] Hence, the application of corrosion-protective coatings is necessary. For example, environmental barrier coatings (EBCs) with a thickness of approximately 100 μm are commonly employed to protect ceramic matrix composite (CMC) components, such as SiC/SiC, in aircraft jet engines from high-temperature oxidation environments.[10] On the other hand, coatings for nuclear reactor-related components must be as thin as possible to maintain thermal conductivity and neutron economy. Therefore, research efforts are underway to develop surface coatings using metals or their compounds such as Ti, Cr, ZrC, CrN, TiN, and ZrN.[11-15] However, delamination of these coatings has been reported after neutron irradiation, primarily on account of the differences in the volume expansion induced by neutron irradiation between the metal coatings and SiC. Since the optimal approach comprises applying coatings to ceramic substrates with comparable irradiation behaviors, some research is being carried out to develop corrosion-resistant ceramic coatings, such as dense SiC deposited by chemical vapor deposition (CVD) and oxide ceramics of approximately 15 μm thick.[16,17]

To develop ceramic coatings, it is crucial to evaluate the strength of the coatings themselves. For example, the fuel cladding tube is subjected to highly concentrated biaxial stress owing to pellet-cladding mechanical interaction (PCMI), highlighting the importance of assessing the strength of the coating under such stress conditions. Tensile testing is the most direct method of investigating the mechanical properties of thin films. Previous assessments of thin SiC film strengths have attempted to evaluate mechanical properties such as tensile strength, elastic modulus, and stress-strain data, even attempting to obtain their elastic moduli through biaxial tensile testing.[18-21] Previous assessments of thin SiC film strengths have attempted to evaluate mechanical properties such as tensile strength, elastic modulus, and stress-strain data, even attempting to obtain their elastic moduli through biaxial tensile testing. However, handling very thin test specimens presents challenges that compromise the reproducibility of the results. In addition to tensile testing, alternative methods, such as nanoindentation, bulge testing, and bending testing using cantilever test specimens, have been employed to evaluate the mechanical properties of thin films.[22-24] Nonetheless, these methods are often limited to measuring parameters such as the elastic modulus, hardness, and fracture toughness at very specific location, and directly determining the fracture strength of an area with a certain degree of spread can pose challenges.

In this study, the Ring-on-Ring test was selected to apply biaxial tensile stress to thin films while minimizing the stress concentration at the edge of the specimen. However, when working with thin films with a thickness of several tens of micrometers, accurately measuring their strength solely through the Ring-on-Ring test becomes challenging owing to the significant local deflection that takes places at their loading point. Therefore, the aim of this study is to establish a method for evaluating the strength of thin SiC coatings using a Ring-on-Ring test by incorporating a graphite substrate as a stress transmission intermediary between the load ring and the coating. In this study, the results obtained from coatings of varying thicknesses were compared to validate the obtained strength values. In addition, the results were compared with those reported in previous studies involving similar materials.

2. Experimental procedure

The SiC coating was synthesized using a cold-wall-type Chemical Vapor Deposition (CVD) system equipped with a high-output fiber laser (wavelength: 1080 nm, maximum output: 500 W). Graphite disks (IGS-

743, φ10×1.0^{t} mm, Shin Nippon Techno Carbon, Japan) were utilized as substrates for the deposition process. The CVD-SiC precursor employed was hydridopolycarbosilane (CVD-4000, Starfire Systems Inc., U.S.), which was evaporated at a temperature of 60 ℃ and introduced into the chamber with an Ar carrier gas at a flow rate of 100 sccm. Throughout the CVD process, the surface temperature of the substrate was monitored continuously using an infrared thermometer. The temperature of the gas-outlet nozzle was maintained at a constant value of 250 ℃ by a heater wound around the nozzle, while the substrate temperature was controlled at 1050 ℃ by adjusting the laser output. The chamber pressure ranged from 200 to 400 Pa during the deposition step. The deposition time was varied between 3 and 20 min, depending on the desired coating thickness. Subsequently, the laser output was decreased to lower the substrate temperature to approximately 500 ℃, followed by air-cooling the substrate to room temperature. The residual stress within the SiC coating was determined from the curvature of a selected specimen using Stoney's equation[25]. It should be noted that the curvature measurement was performed on the surface of a strip specimen cut to dimensions of 1 mm × 1 mm × 10 mm, since the curvature of the as-coated disc specimens was below the detection limit. The Young's modulus of the SiC coating was determined through nanoindentation testing (G200, Agilent Technologies, U.S.) performed at room temperature.

In this study, the load and support rings, as shown in Figures 1a and b, were used in accordance with the ASTM C1499 standard.[26] The diameters of the load ring and the support ring were 4.5 mm and 9 mm, respectively, with both rings having a curvature radius of 0.4 mm. The fixtures were made of SUS304 and the contact ball was made of silicon nitride. The strength tests were conducted at room temperature using a conventional testing machine (model 210X, INTESCO Co., Ltd., Japan), at a testing speed of 0.05 mm/min. The coating surface was placed facing downwards to apply equi-biaxial tensile stress, as shown in Figure 1b. Figure 1c shows the stress distributions estimated using the Finite Element Method (FEM) for a SiC coating with a thickness of 10 μm coated on a graphite substrate, where the specimen was subjected to an 80 N load by the Ring-on-Ring test. Figure 1d shows the results of the cross-section FEM analysis of said thin-film under the conditions shown in Figure 1c. An Autodesk Inventor Nastran was used for the FEM analysis, and the modulus of each material was determined using the values measured with the nanoindenter described above. The

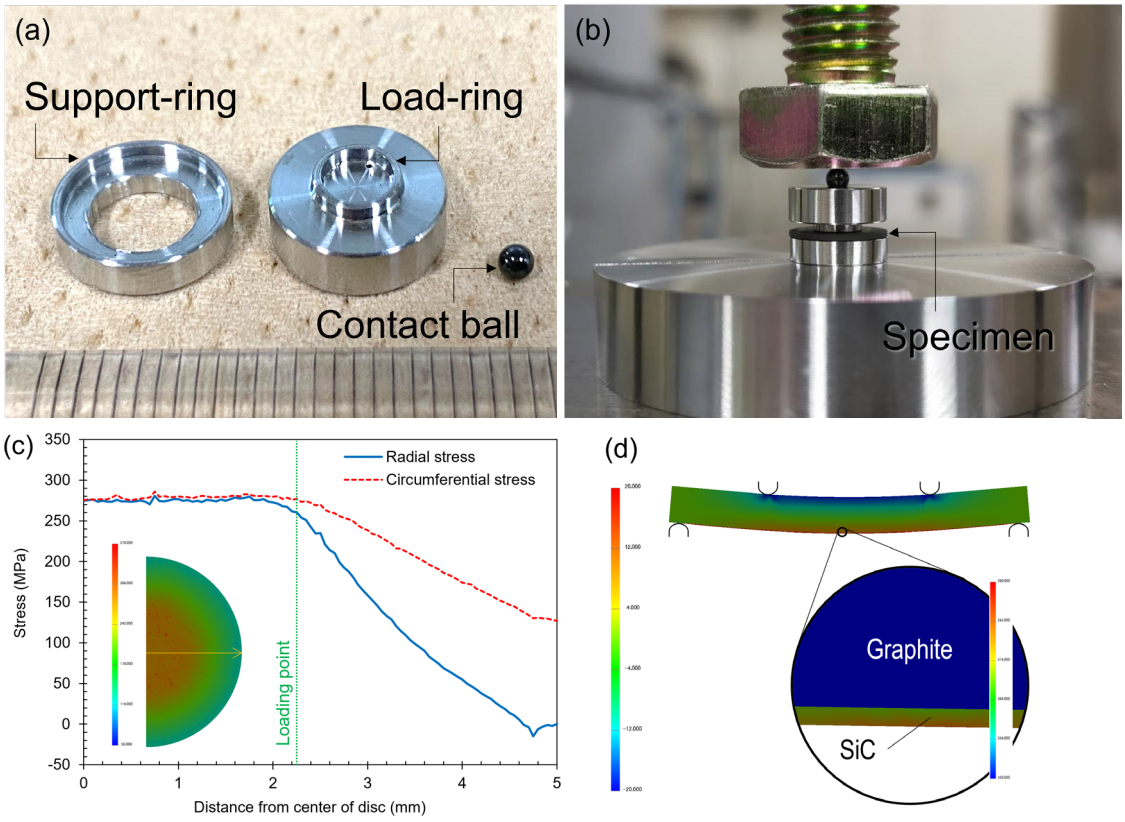

FIGURE 1 Overview of the Ring-on-Ring testing; (a) test fixtures, (b) specimen during loading, (c, d) FEM results of the loading stress distribution in the SiC coating.

Poisson's ratios for the SiC, graphite, and SUS304 fixtures were set to 0.21, 0.2, and 0.3, respectively. Second-order tetrahedral elements were employed as the element type, and separate contact conditions were used to model the interactions between the components. As the optimization of the graphite thickness was the primary focus of the FEM analysis, the residual stresses within the film were not considered. The analysis confirmed that there was no stress concentration directly under the load ring under any of the conditions tested in this study.

The equi-biaxial stress for a bilayer material during the Ring-on-Ring test was analytically derived by Huseh et al., as shown in equation (1).[27]

$$\sigma = \frac{-PE_1(z - z_n^*)}{8\pi(1 - \nu_1^2)D^*}\left[2(1+\nu)\ln\left(\frac{a}{b}\right) + \frac{(1-\nu)(a^2 - b^2)}{R^2}\right] \quad (1)$$

, where P is the applied load, E_1 and ν_1 are the Young's modulus and Poisson's ratio of the SiC coating, respectively, a and b are the diameters of the load and support rings, respectively, and z is the height, measured from the bottom surface of the specimen. z_n^* and D^* represent the neutral-plane position and bending rigidity of the two-layer disk, respectively, and are expressed by equation (2) and (3), respectively. v is the average Poisson's ratio given by equation (4).

$$z_n^* = \frac{E_1\, t_1^2/2\,(1-\nu_1^2) + E_2\, t_2^2/2\,(1-\nu_2^2) + E_2 t_1 t_2/(1-\nu_2^2)}{E_1\, t_1/(1-\nu_1^2) + E_2\, t_2/(1-\nu_2^2)} \tag{2}$$

$$D^* = \frac{E_1 t_1^3}{3(1-\nu_1^2)} + \frac{E_2 t_2^3}{3(1-\nu_2^2)} + \frac{E_2 t_1 t_2 (t_1+t_2)}{1-\nu_2^2} - \frac{[E_1\, t_1^2/2\,(1-\nu_1^2) + E_2\, t_2^2/2\,(1-\nu_2^2) + E_2 t_1 t_2/(1-\nu_2^2)]^2}{E_1\, t_1/(1-\nu_1^2) + E_2\, t_2/(1-\nu_2^2)} \tag{3}$$

$$v = \frac{\nu_1 t_1 + \nu_2 t_2}{t_1 + t_2} \tag{4}$$

, where E_2 and ν_2 represent the Young's modulus and Poisson's ratio of the graphite substrate, respectively, and t_1 and t_2 represent the thicknesses of the SiC coating and graphite substrate, respectively.

Continuous in-situ imaging of the coating fracture during the test was recorded at a frame rate of 30 fps. through a hole (φ6 mm) in the support ring (Figure 1a) using a digital microscope (RH-8800, Hirox Co., Ltd., Japan). The instant of crack initiation was identified through digital image correlation (DIC) analysis using the GOM Correlate software (Carl Zeiss GOM Metrology GmbH, Germany).

3. Results and discussion

The X-ray diffraction (XRD) results of the SiC coating on the graphite substrate are presented in Figure 2. In addition to the peaks originating from the graphite substrate, a broad peak at 2θ = 36° corresponding to the (111) reflection plane of CVD-SiC was observed, indicating the presence of an amorphous or low-crystallinity SiC film. To quantify the residual stress, the curvatures of the as-coated disk-shaped samples that remained below the detection limit of the laser microscope were evaluated. However, upon slicing the center into approximately 1 mm wide strips, with the aim of emphasizing the radial stress, an extremely subtle curvature was observed. As an example, the residual stress for a specimen coated with a 5.1 μm SiC film was

estimated to be 153 ± 15 MPa. Although, in the case of specimens with thicker coatings, the curvature remained undetectable even after the stripping process, these specimens could contain some residual stress because the strain mismatch between the coating and the substrate was the primary source of such residual stress. Assuming that this stress is uniformly distributed throughout the thickness of the as-coated films, it can be inferred that the residual stress exhibits an inverse relationship with the film thickness. Consequently, in the subsequent results, the fracture stress was corrected by incorporating the corresponding film thickness for each specimen based on the measured residual stress indicated above.

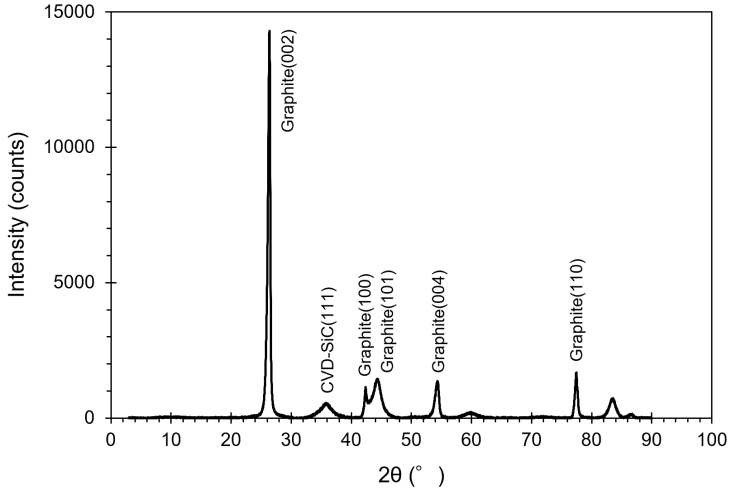

FIGURE 2 XRD pattern of as received SiC coating chemically deposited on the graphite substrate.

Figures 3a–c show the optical microscope images of the fractured specimens taken from the coating side and the SEM images of the specimen cross-section surrounding the crack origin determined by DIC. Based on the optical microscope images, it was observed that cracks propagated in a somewhat radial manner from the crack origin. The crack origin was consistently found within the loading area for all specimens. These observations suggest an absence of stress concentration directly beneath the loading point, indicating that the specimens were subjected to a uniform and equi-biaxial tensile stress. No delamination between the coating and

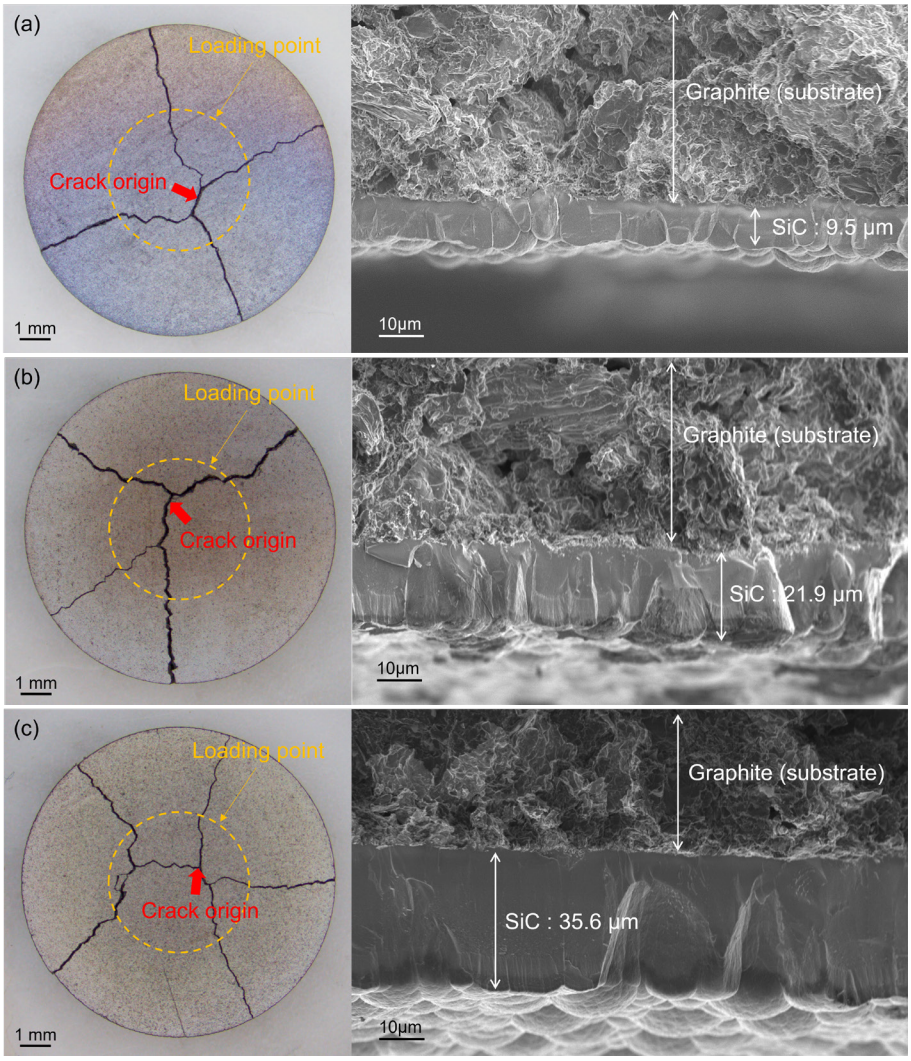

FIGURE 3 Typical OM images of the coated faces after testing and SEM images of the fractured surface; film thickness of (a) 9.5 μm, (b) 21.9 μm, (c) 35.6 μm.

the substrate was observed at the fractured cross-sections of all specimens. Moreover, the coatings exhibited no detectable pores at the magnification level utilized, indicating the successful fabrication of a dense SiC coating on the graphite substrate. The SEM images did not provide clear indications of the crack origin in any of the specimens. However, two distinct types of fracture morphologies were observed on the surfaces: fracture along the grain boundaries and smooth surfaces likely indicating intragranular fracture.

Figure 4 shows typical DIC images indicating the color map of the maximum principal strains on the coated surface. These images show a 6 mm diameter region at the center of the specimen, which is approximately within the diameter of the load ring. Notably, these DIC images correspond to the same specimen, as shown in Figure 3a. The strain gradually accumulated in an island-like pattern, as observed in the images captured at 89 (Figure 4B) and 116 sec. (Figure 4C) of testing time. With time, a localized strain concentration gradually formed at a specific point, as indicated by the arrow in Figure 4C. In most cases, this particular point was found to be the site of initiation of the first crack. It is worth noting that in less common cases where

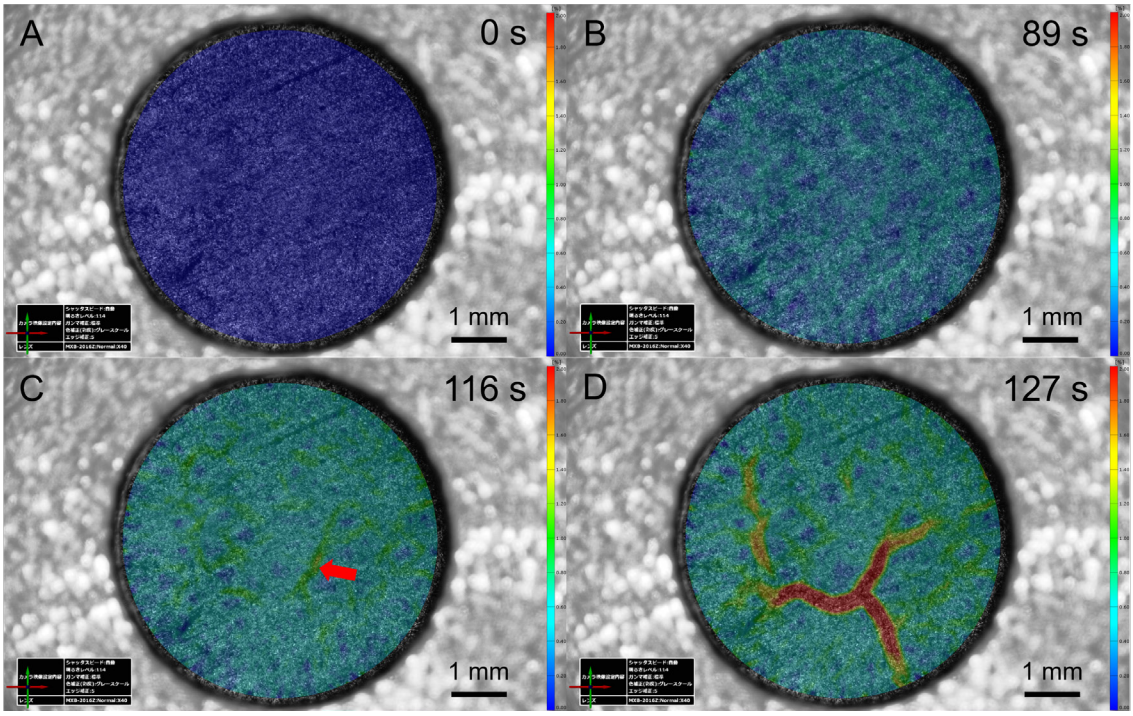

FIGURE 4 DIC images showing the maximum principal strain of the coated face during the test.

multiple stress concentration points occurred simultaneously, the stress was concentrated at any one of these points before cracking occurred, whereas the stress concentration at the other points could dissipate. As the crack propagated, it branched off and extended toward the outer edge of the specimen (Figure 4D).

To determine the time at which the crack started to form, the distance between two points perpendicular to it was continuously measured on continuous DIC images, starting at t=0 sec., as shown in Figure 5 (blue line). The average maximum principal strain within the loading area is plotted against testing time in Figure 5 (green line), it presents the results of the identical specimens shown in Figures 3a and 4. The symbols A to D on the blue line in Figure 5 correspond to the times shown in Figures 4A– and D, respectively. As the testing time increases, the distance between the two points increases linearly. However, when the testing time reaches 116 sec. (Figure 5C), said distance shows a dramatic increase that deviates from the expected linear increase. This suggests the formation of a crack in the coating at that time, which is defined as the crack initiation time in this study. However, the average maximum principal strain continued to increase linearly after the crack

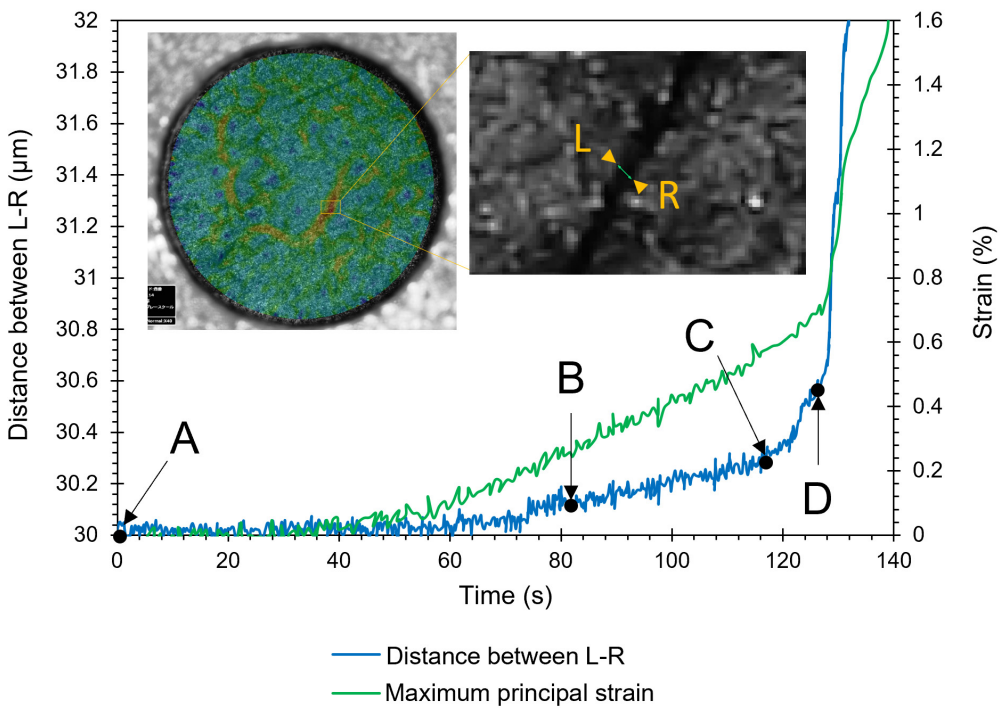

FIGURE 5 The distance between L-R and the average maximum principal strain within the loading area analyzed by DIC. Inset images indicate the positions of the two points perpendicular to the crack.

initiation. Finally, the graphite substrate fractured after 127 sec. (Figure 5D), which led to a rapid increase in the average strain. Because the SiC coating was applied to the graphite substrate, even if cracks occurred in the SiC coating, the film specimen was not immediately separated until the substrate fractured. Therefore, when the crack opening rate became nonconstant, the strength of the coating was calculated using the load applied at 116 sec. and equation (1).

The results of the equi-biaxial strength of the SiC coating, calculated using equation (1) and corrected by

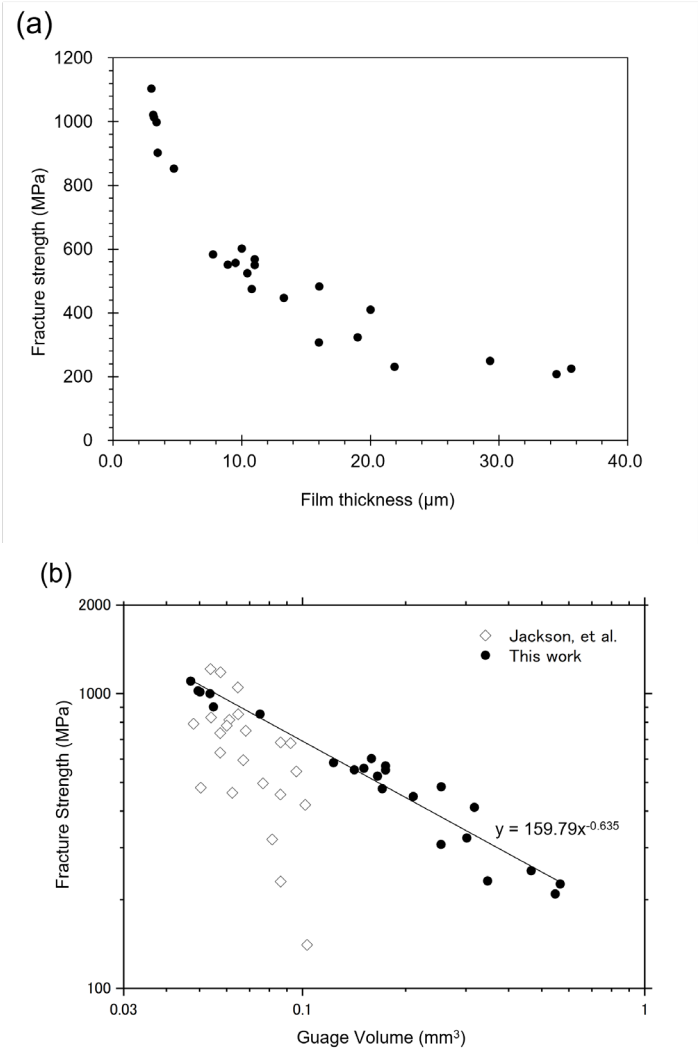

FIGURE 6 Equi-biaxial strength of SiC coatings; (a) dependence on film thickness, (b) dependence on gauge volume.

the results of the residual stress measurements, are shown in Figure 6a. The strength and residual stress of each specimen are summarized in Table 1. The Young's moduli of the SiC coating and graphite substrate were measured as 268 GPa and 10.8 GPa, respectively, using a nanoindenter. The Poisson's ratio values were found to be 0.20 for the SiC coating and 0.21 for the graphite substrate. The equi-biaxial strength of the SiC coating decreased with increasing the film thickness, and this decrease seems to be constant beyond the 22 μm thickness. In ceramic materials, the specimen size significantly affects strength; a similar phenomenon was observed in this study, in which the fracture strength of the SiC coating decreased with increasing specimen volume. This can be attributed to the higher probability of defects as the specimen volume increases, which act as initiation points for fracture, ultimately leading to a reduction in fracture strength. Moreover, the results suggested that the strength of the coatings was influenced more by the specimen volume rather than by surface conditions. This implies that the coatings fractured under tensile rather than bending stresses.

The equi-biaxial tensile strength of the SiC coatings obtained in this study was compared with the uniaxial tensile strength of 3C-SiC micro-samples previously reported in the available literature[18]. Figure 6b illustrates the relationship between the strength, specimen gauge volume, and thin-film volume inside the load ring on a logarithmic scale. According to the Weibull statistical theory,[28] the fracture strength of ceramic materials follows a simple power law with respect to specimen size; the results of this study confirm that strength decreases according to this power law. Within the volume range of small specimens (~0.1 mm^3), the values obtained in

TABLE 1 Coating thickness, residual stress, and strength values of the specimens.

Film thickness (μm)	Residual stress (MPa)	Fracture strength (MPa)	Film thickness (μm)	Residual stress (MPa)	Fracture strength (MPa)
3	265	1104	11	71.4	550
3.1	252.2	1022	11	71.4	569
3.2	248.9	1014	13.2	59.3	448
3.4	232.6	999	16	49.1	308
3.5	227.4	902	16	49.1	483
4.7	166.1	853	19	41.3	324
7.8	101.3	583	20	39.2	411
8.9	88.1	551	21.9	35.9	232
9.5	82.6	558	29.3	26.8	251
10	78.5	603	34.5	22.8	209
10.4	75.4	525	35.6	22	226
10.8	72.9	476			

this study were comparable to the previously reported values. This was likely due to the small size of the specimens, which resulted in a limited number of defects available as potential fracture initiation points. Although the total number of specimens tested in this study was smaller than those in the previous study, the obtained strengths covered a wider range of specimen volumes, and the deviation from the power-law line was smaller, as shown in Figure 6b. The smaller variability in the obtained strength, compared to the previous study, suggests a fewer number of potential fracture initiation points, on account of the lower defect density in the SiC coatings fabricated in this study. In addition, the lower variability in the obtained strength is attributed to the elimination of edge effects. The fracture of brittle materials is largely influenced by stress concentration at the edge defects, leading to different strength values for the same specimen owing to variations in edge conditions.[29] In contrast, biaxial tests, such as Ring-on-Ring tests minimize the stress at the edges of disk specimen. Furthermore, we suggest that the variability in the obtained strength values was lower than the previous study on account of the strength assessment in the biaxial tests being less dependent on the orientation of the cracks than the corresponding assessment in uniaxial tests. Note that the difference in strength between both studies around a specimen volume of 0.1 mm^3 could be attributed to the potential underestimation of strength values in the previous study. Indeed, the previous study estimated residual tensile stress at approximately 200 MPa due to the limitation of preparation methods for specimens with volumes of approximately 0.06 mm^3 or more; residual stress effects on the results were not considered. In addition, the strength of the amorphous SiC coatings approached 220 MPa (Figure 6a). Considering that the tensile strength of crystalline CVD-SiC is 294 MPa[30] and that amorphous SiC generally has a lower strength than crystalline SiC,[31] it can be concluded that the strength of specimens with a film thickness of over 30 μm can be considered as the bulk material strength rather than the thin-film strength in the testing configuration used here.

4. Conclusions

In this study, a new method was developed to evaluate the strength of thin SiC coatings under biaxial tensile stress using a Ring-on-Ring test. A graphite substrate was used as an intermediary to transmit the stress from the load ring to the coating. Crack initiation time and the corresponding load were identified by continuously measuring the crack opening in the SiC coating using DIC analysis. The obtained equi-biaxial

tensile strengths of the SiC coatings were dependent on film thickness, in accordance with the well-known specimen-size effect. The relationship between the fracture strength and specimen size obtained in this study is valid since it follows the typical power law of the size effect in ceramics. Moreover, the lower variability in the strength obtained in this study compared with previous studies is believed to be mainly due to the use of a biaxial test. The results are comparable to the SiC coating strengths previously reported for small specimen volumes and the strength of the thicker specimens approached the bulk strength. Based on the obtained results, it can be concluded that this method allows the evaluation of equi-biaxial strengths in thin films across a broad range of sample sizes.

Acknowledgements

This work was supported by MEXT Innovative Nuclear Research and Development Program Grant Number JPMXD0222682488.

References

[1] Kovalčíková A, Sedláček J, Lenčéš Z, Bystrický R, Dusza J, Šajgalík P. Oxidation resistance of SiC ceramics prepared by different proceessing routes. J Eur Ceram Soc. 2016;36(15):3783–3793.

[2] Hopkins GR, Chin J. SiC matrix/SiC fiber composite: a high-heat flux, low activation, structural material. J Nucl Mater. 1986;141:148-151.

[3] Wang P, Liu F, Wang H, Li H, Gou Y. A review of third generation SiC fibers and SiCf/SiC composites. J Mater Sci Technol. 2019;35(12):2743–2750.

[4] Katoh Y, Snead LL, Henager CH, Nozawa T, Hinoki T, Iveković A, et al. Current status and recent research achievements in SiC/SiC composites. J Nucl Mater. 2014;455:387-397.

[5] Iveković A, Novak S, Dražić G, Blagoeva D, Gonzalez de Vicente S. Current status and prospects of SiCf/SiC for fusion structural applications. J Eur Ceram Soc. 2013;33(10):1577-1589.

[6] Koyanagi T, Katoh Y, Nozawa T, Snead LL, Kondo S, Henager CH, et al. Recent progress in the development of SiC composites for nuclear fusion applications. J Nucl Mater. 2018;511:544-555.

[7] Satvik K, Mathur P, Mahawar A, Singh K, Selvaraj SK. Literature survey to the materials used in

laser-assisted additive manufacturing processes for the production of nuclear materials. Eur Phys J Plus. 2021;136(8).

[8] Koyanagi T, Terrani K, Harrison S, Liu J, Katoh Y. Additive manufacturing of silicon carbide for nuclear applications. J Nucl Mater. 2021;543:152577.

[9] Alexander GB, Heston WM, Iler RK. The solubility of amorphous silica in water. J Phys Chem. 1954;58(6):453-455.

[10] Suzuki M, Shahien M, Shinoda K, Akedo J. The Current Status of Environmental Barrier Coatings and Future Direction of Thermal Spray Process. Mater Trans. 2022;63(8):1101-11.

[11] Doyle PJ, Koyanagi T, Ang C, Snead L, Mouche P, Katoh Y, et al. Evaluation of the effects of neutron irradiation on first-generation corrosion mitigation coatings on SiC for accident-tolerant fuel cladding. J Nucl Mater. 2020;536:152203.

[12] Raiman SS, Doyle P, Ang C, Katoh Y, Terrani KA. Hydrothermal corrosion of coatings on silicon carbide in boiling water reactor conditions. Corrosion. 2019;75(2):217-223.

[13] Ueta S, Aihara J, Yasuda A, Ishibashi H, Takayama T, Sawa K. Fabrication of uniform ZrC coating layer for the coated fuel particle of the very high temperature reactor. J Nucl Mater. 2008;376(2):146-151.

[14] Ishibashi R, Ishida K, Kondo T, Watanabe Y. Corrosion-resistant metallic coating on silicon carbide for use in high-temperature water. J Nucl Mater. 2021;557:153214.

[15] Ishibashi R, Hayashi Y, Bo H, Kondo T, Hinoki T. Radiation Effect in Ti-Cr Multilayer-Coated Silicon Carbide under Silicon Ion Irradiation up to 3 dpa. Coatings.2022;12(6):832.

[16] Kim D, Lee HG, Park JY, Kim WJ. Fabrication and measurement of hoop strength of SiC triplex tube for nuclear fuel cladding applications. J Nucl Mater. 2015;458:29-36.

[17] Usukawa R, Katsui H, Shimoda K, Kondo S, Hotta M. Microstructure and integrity of multilayer ceramic coating with alumina top coat on silicon carbide by laser chemical vapor deposition. Ceram Int. 2023;49(7):10946-10952.

[18] Jackson KM. Fracture strength, elastic modulus and Poisson's ratio of polycrystalline 3C thin-film silicon carbide found by microsample tensile testing. Sens Actuators A Phys. 2005;125(1):34-40.

[19] Mehregany M, Tong L, Matus LG, Larkin DJ. Internal stress and elastic modulus measurements on micromachined 3C-SiC thin films. IEEE Trans Electron Devices. 1997;44(1):74-79.

[20] Leisen D, Rusanov R, Rohlfing F, Fuchs T, Eberl C, Riesch-Oppermann H, et al. Mechanical characterization between room temperature and 1000° C of SiC free-standing thin films by a novel high-temperature micro-tensile setup. Rev Sci Instrum. 2015;86(5)055104.

[21] Taechung Y, Li L, Kim CJ. Microscale material testing of single crystalline silicon: process effects on surface morphology and tensile strength. Sens Actuators A Phys. 2000;83(1-3):172-178.

[22] Roy S, Zorman C, Mehregany M, DeAnna R, Deeb C. The mechanical properties of polycrystalline 3 C-SiC films grown on polysilicon substrates by atmospheric pressure chemical-vapor deposition. J Appl Phys. 2006;99(4):044108.

[23] Maruthoor S, Ajayakumar A, Fuchs T, Jakovlev O, Reinecke H, Wilde J. Mechanical Characterization of Polycrystalline and Amorphous Silicon Carbide Thin Films Using Bulge Test. J Microelectromech Syst. 2013;22(1):140-6.

[24] Xiaodong L, Bhushan B. Micro/nanomechanical characterization of ceramic films for microdevices. Thin solid films. 1999;340(1-2):210-217.

[25] Stoney GG. The tension of metallic films deposited by electrolysis. Proc Math Phys Eng Sci. 1909;82(553):172-5.

[26] Standard Test Method for Monotonic Equibiaxial Flexural Strength of Advanced Ceramics at Ambient Temperature. Standard ASTM C1499-04, West Conshohocken, 2005.

[27] Hsueh CH, Luttrell CR, Becher PF. Analyses of multilayered dental ceramics subjected to biaxial flexure tests. Dent Mater. 2006;22(5):460-469.

[28] Bažant ZP. Size effect on structural strength: a review. Arch Appl Mech. 1999;69(9-10):703-25.

[29] Lo WC. Edge Effect on the Modulus of Rupture of Ceramic Substrates. The Science of Ceramic Machining and Surface Finishing. 1972;348:399.

[30] Ferrotec Material Technologies Corporation. CVD-SiC(Chemical Vapor Deposition Silicon Carbide) | Ferrotec Material Technologies Corporation. [homepage on the Internet]. [cited 2023 Apr 29]. Available from: https://ft-mt.co.jp/en/product/semiconductor_equipment/cvd_sic/

[31] Yuan X, Kondo S, Yabuuchi K, Yu H, Ogino Y, Kasada R. Effects of grain boundary volume fraction on the threshold dose of irradiation-induced SiC amorphization at 30° C. J Eur Ceram Soc. 2023;43(12):5125-5135.

Figure Captions

FIGURE 1

Overview of the Ring-on-Ring testing; (a) test fixtures, (b) specimen during loading, (c, d) FEM results of the loading stress distribution in the SiC coating.

FIGURE 2

XRD pattern of as received SiC coating chemically deposited on the graphite substrate.

FIGURE 3

Typical OM images of the coated faces after testing and SEM images of the fractured surface; film thickness of (a) 9.5 μm, (b) 21.9 μm, (c) 35.6 μm.

FIGURE 4

DIC images showing the maximum principal strain of the coated face during the test.

FIGURE 5

The distance between L-R and the average maximum principal strain within the loading area analyzed by DIC. Inset images indicate the positions of the two points perpendicular to the crack.

FIGURE 6

Equi-biaxial strength of SiC coatings; (a) dependence on film thickness, (b) dependence on gauge volume.

TABLE 1

Coating thickness, residual stress, and strength values of the specimens.